Installation, Calibration, and Experimental Verification of a Layered Deposition Scheme

Julian Calder

Office of Science, Science Undergraduate Laboratory Internship Program

Middlebury College, Middlebury, VT

National Renewable Energy Laboratory

Golden, Colorado

August 12, 2022

Prepared in partial fulfillment of the requirement of the Department of Energy, Office of Science's Science Undergraduate Laboratory Internship Program under the direction of Rebecca Smaha at the National Renewable Energy Laboratory.

Participant: Julian Calder

Mentor: Rebecca Smaha

ABSTRACT

Radio frequency magnetron sputtering provides a simple yet effective method with which to produce thin films of a wide variety of materials. Many sputtering chambers utilize co-deposition, in which multiple materials are deposited onto a substrate simultaneously. With increasingly modernized sputtering chambers, though, the ability to independently control and automate the shutter mechanisms of individual sputtering guns allows for the possibility of producing layered films in-situ. Here, layered material deposition is explored through the installation of in situ rate/thickness calibration tools, followed by the synthesis and characterization of layered magnesium tungsten nitride ($MgWN_2$) by means of an automated shutter program. Quartz crystal monitors are installed and calibrated to determine material deposition rate, from which shutter duration is calculated to produce desired layer thicknesses. X-ray diffraction (XRD) and X-ray fluorescence (XRF) data reveal film structure and composition, while X-ray reflectometry (XRR) measures film thickness and confirms the existence of material layering. These preliminary results show that this method of layered material deposition has the potential to produce numerous previously undiscovered materials and may, with further revisions such as varying substrate temperature, material, and capping layer thickness, provide the ability to create novel heterostructured crystalline materials.

I. INTRODUCTION

Interest in 2-dimensional heterostructures has grown exponentially since the initial discovery of monoatomic-layer graphene in 2004.[3] Layered heterostructures comprised of a series of stable 2D crystal layers joined together by van der Waals forces present an exciting new class of material with promising applications to numerous technologies including novel semiconductors, solar cells, and high-efficiency LEDs.[1,4] These 2D materials allow for significant tunability of electronic properties by varying composition, layer thicknesses, overall material thickness, and other physical characteristics.[4]

Research at the National Renewable Energy Laboratory on van der Waals heterostructures has focused primarily on the development of sulfide heterostructure amorphous chemical precursors by means of sputter deposition.[5] The goal of these precursors was to deposit the necessary number of atoms needed to form a series of amorphous or nanocrystalline monolayer constituents which will, under a gentle heating process, reorganize into the desired crystalline heterostructure.[5] Researchers were able to successfully produce sulfide heterostructure precursors of SnS-MoS_2 and SnS-TaS_2 that self-assembled at low annealing temperature into ordered crystalline superlattices.[5,6]

Synthesis of layered heterostructures via sputtering requires the ability to independently control material deposition from individual sputtering guns to allow for precise layer-specific thicknesses. Nearly all sputtering chambers contain some way to regulate material deposition, typically in the form of metal shutters that cover the sputtering guns themselves, but these shutters are not usually controllable in such a way conducive to making a multi-layered superstructure of different materials.

In this project, we enable the deposition of layered heterostructural materials in a new, digitally-controlled sputtering chamber. As a test case, we attempt to grow layered $MgWN_2$, a novel material of interest which has been observed to form an ordered, layered crystalline structure under certain annealing conditions.[8] To achieve this, we installed quartz crystal monitors and calibrated the deposition rates through a series of Mg_xN_y and W_xN_y growths. We extracted optimal shutter times from these calibration growths and used them in an automated shutter program.

This paper will begin by discussing the process of installing and calibrating the quartz crystal monitors within the sputtering chamber and verifying that layered material deposition is present. Then, we will transition to discussing the synthesis of layered $MgWN_2$ and explore the viability of this automated shutter program in producing other potential layered superstructures in-situ.

II. METHODS

The process of producing layered thin films occurred in three primary steps: 1) Installation and calibration of the quartz crystal monitors to provide accurate material deposition information. 2) Application of the calibrated deposition information to produce layered $MgWN_2$ thin films. 3) Running a series of characterization tests on the $MgWN_2$ films to determine crystal structure, chemical composition, and material layering.

A. Sensor Calibration

1. Sensor Installation

Four INFICON quartz crystals were installed into individual sputtering sensors positioned above each sputtering gun within the chamber adjacent to the substrate as shown in Figure 1. Individual inflow and outflow water cooling lines were also connected in parallel to each sensor to allow for high-temperature material deposition without compromising sensor integrity (see Figure 2).

2. Software Configuration

Following installation, the quartz crystal monitors were connected to an INFICON SQM-160 Thin Film Deposition Monitor to allow for individual sensor-by-sensor data logging and parameter adjustment. Within the film configuration menu, the density and z-ratio parameters were selected based on tabulated values for Mg and W provided by INFICON. The density of sensor 2 (positioned above Mg gun) was set at 1.74 g/cm^3 with a z-ratio of 1.610. The density of sensor 4 (positioned above W) was set at 19.3 g/cm^3 while the z-ratio was 0.163. Tooling factors were then adjusted based on results of the subsequent calibration growths.

3. Calibration Growths

A series of calibration growths were performed in which either magnesium nitride (Mg_3N_2) or tungsten nitride (WN_x) were deposited on a rotating EXG glass substrate under identical

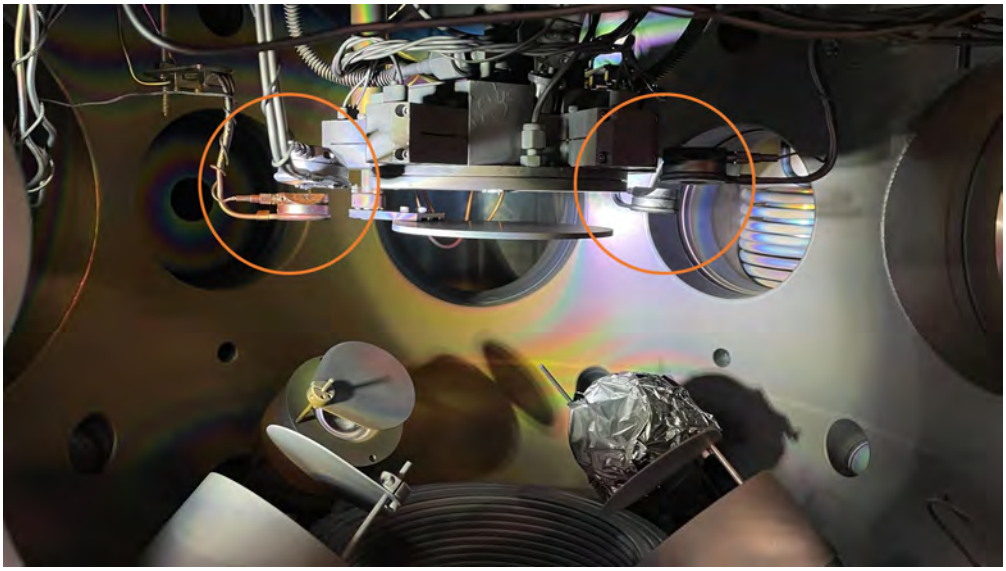

Figure 1: Interior of sputtering chamber, showing four quartz crystal sensors circled in orange.

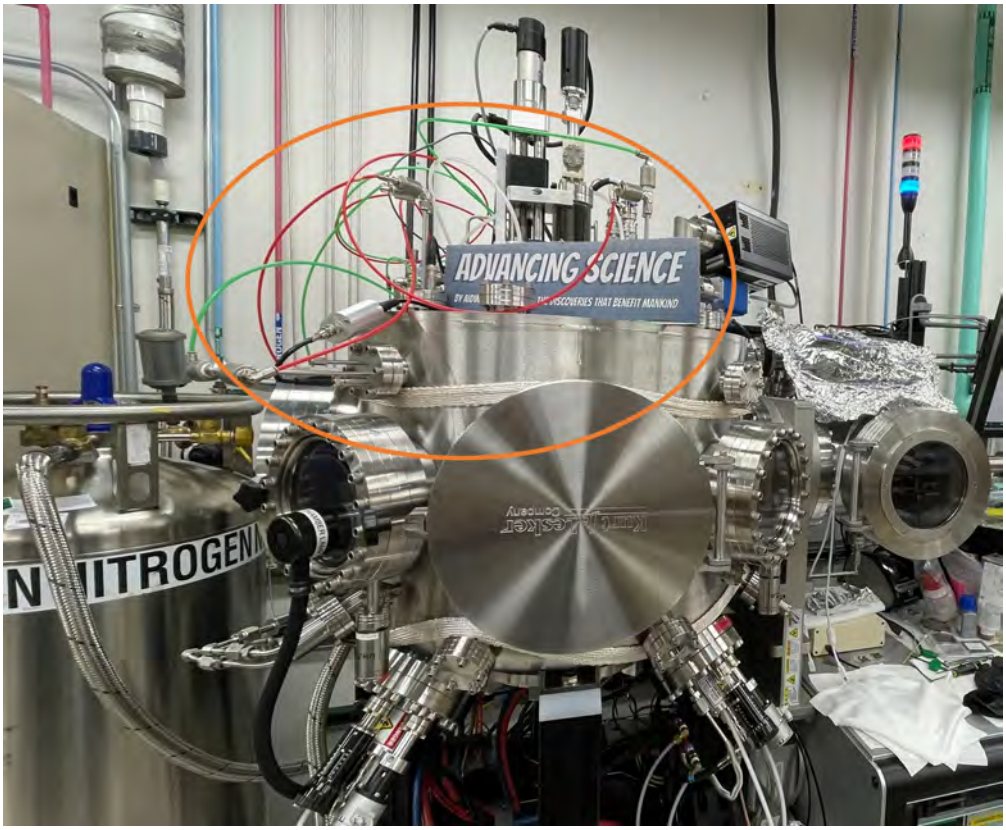

Figure 2: Exterior of sputtering chamber, showing water cooling lines connected to each individual quartz crystal monitor circled in orange.

deposition conditions (25 sccm Ar flowing to each gun with 50 sccm N_2 flowing to the substrate, chamber pressure of 8.1 mTorr). Film thicknesses were measured by a profilometer as described in the characterization methods section below and used to calibrate QCM results. Tooling factor values were generally adjusted after each growth, and compared to profilometer measurement of subsequent growth. See Table 1 for calibration growth deposition information.

Sample Number	Deposition Time	Mg/W Gun Powers	Chamber Pressure
182	90 min.	120 W Mg	8.1 mTorr
183	90 min.	120 W W	8.1 mTorr
184	90 min.	120 W Mg	8.1 mTorr
185	90 min.	120 W W	8.1 mTorr
186	90 min.	120 W Mg	8.1 mTorr
187	90 min.	120 W W	8.1 mTorr
188	90 min.	120 W Mg	8.1 mTorr

Table 1: Deposition parameters for Mg_3N_2 and WN_x calibration growths including deposition time, gun powers, and chamber pressure. Note that all samples were grown on EXG glass and rotated, to decrease variance in thickness across the film.

B. $MgWN_2$ Growths

Sample libraries were grown using RF magnetron co-sputtering from elemental metallic targets of Mg (99.98%) and W (99.95%) in a reactive nitrogen atmosphere. A gradient of the Mg–W cations was intentionally grown in a nitriding environment to observe correlations between stoichiometry and phases present. The gun powers are tabulated in Tables 1-2. Base pressure in the chamber was between $3.5 * 10^{-8}$ and $6.7 * 10^{-7}$ Torr, and a liquid nitrogen cryoshroud was generally used to minimize water vapor near the substrate. The chamber pressure was 10.6 mTorr during deposition, with 50 sccm of flowing Ar and 50 sccm of flowing N_2. The substrate was usually kept at ambient temperature during deposition, although the effect of deposition temperature was probed (see deposition parameters in 2). The substrates were 50.8×50.8mm squares of EXG glass, pSi(100), or 100 nm LCPVD-grown SiN_x on Si (University Wafers). Select samples grown on SiN_x | Si substrates were capped with a 30 min deposition (∼25 nm) of sputtered AlN without breaking vacuum to protect against oxidation (see Tables 1-2). Layered films were grown with an automated shutter program with gun-specific shutter times and a set number of cycles to allow for precise deposition of different materials.

C. Characterization Methods

Experimental combinatorial data used by this study have been analyzed using the COMBIgor software package.[7] Cation composition was measured with X-ray fluorescence (XRF) using a Bruker M4 Tornado under vacuum (∼15 mTorr). The cation ratio was mapped across sample libraries.

Sample Number	Deposition Time	Mg/W Gun Powers	Substrate Material	AlN Capping Layer
179	120 min.	60/60 W	EXG	None
180	120 min.	60/65 W	EXG	None
181	120 min.	120/130 W	EXG	None
189	120 min.	120/130 W	pSi	None
196	30 min.	120/130 W	pSi	None
198	120 min.	120/130W	SiN_x | Si	30 min. AlN

Table 2: Deposition parameters for non-layered $MgWN_2$ growths, including sample number, deposition time, gun powers, and substrate material. Note that chamber pressure was maintained at 10.6 mTorr for every non-layered growth.

Sample Number	Mg/W Shutter Times	Number of Cycles	Mg/W Gun Powers	Substrate Temperature	Substrate Material	AlN Capping Layer
191	8s/9s	400	120/130 W	Ambient	pSi	None
192	8s/9s	400	120/130 W	200 °C	pSi	None
194	8s/9s	400	120/130 W	400 °C	pSi	None
195	8s/9s	100	120/130 W	Ambient	pSi	None
197	16s/18s	50	120/130 W	Ambient	pSi	None
199	8s/9s	100	120/130 W	Ambient	SiN_x | Si	30 min AlN
200	80s/90s	10	120/130 W	Ambient	pSi	None
201	8s/9s	400	120/130 W	Ambient	pSi	None
202	40s/45s	20	120/130 W	Ambient	pSi	None
203	32s/36s	25	120/130 W	Ambient	pSi	None
204	24s/27s	33	120/130 W	Ambient	pSi	None

Table 3: Deposition parameters for layered $MgWN_2$ growths, including sample number, Mg/W shutter times, number of cycles, gun powers, and substrate material. Note that chamber pressure was maintained at 10.6 mTorr for all layered growths.

Calibration thickness data were collected under atmospheric conditions using a Veeco Dektak 8 profilometer with a 5 μm stylus radius. Thickness data were mapped across sample libraries and averaged to determine best-fit thickness.

Laboratory X-ray diffraction (XRD) data were collected with Cu K_α radiation using a Bruker D8 Discover equipped with a 2D detector that allowed spatial mapping across the sample library. X-ray reflectivity (XRR) patterns were collected on select samples with Cu K_α radiation on a Rigaku Smartlab equipped with parallel beam optics and a Ge(220) monochromator.

Rapid thermal annealing (RTA) studies were performed on single rows of sample libraries at a range of temperatures under 8 slpm flowing N_2 in a ULVAC MILA-3000 RTA furnace. The RTA procedure consisted of a three min hold at 100 °C, a one min ramp to the set temperature (600 °C, 800 °C, or 900 °C), and a hold at the set temperature for 3 min, followed by rapid cooling to room temperature. Each anneal was followed by laboratory

XRD as described above.

III. RESULTS AND DISCUSSION

A. Calibration Process

Calibration growth thicknesses were measured by a profilometer twice following deposition and were then compared to QCM thickness data to determine necessary parameter adjustment for agreement between QCM and profilometer data. See Tables 4 and 5 for thickness data.

Sample Number	Measurement 1 Thickness	Measurement 2 Thickness	Average Thickness	QCM Thickness
182	178.46 nm	235.26 nm	206.86 nm	259.6 nm
184	149.13 nm	172.13 nm	160.63 nm	142.5 nm
186	112.27 nm	370.12 nm	241.195 nm	150.6 nm
188	109.58 nm	425.43 nm	267.505 nm	151.4 nm

Table 4: Thickness results for Mg_3N_2 calibration growths. Note that updated density and z-ratio information are reflected in sample number 184, and 186 reflects an updated tooling factor of 105%.

There was substantial discrepancy between the first and second profilometer measurements of the Mg_3N_2 growths, likely due to the immediate oxidation of the film following removal from the chamber as a result of Mg's high affinity for oxygen. While oxidation layers are typically <10 nm in thickness, profilometry data revealed more than 10x that amount of variation, which made it challenging to extract meaningful information from these measurements. Estimations based on subtracting the thickness of WN_x from a combined $MgWN_2$ growth revealed that measurement 1 of sample 184 was likely the most accurate, and thus the tooling factor was adjusted to 105% to yield approximately 150 nm for recorded thickness as it did in samples 186 and 188. This tooling factor yielded a material deposition rate of approximately 0.28 Å/s, though there was likely considerable error in this measurement.

Implementation of a non-oxidizing capping layer (such as AlN) might be an effective method to reduce the oxidation of Mg_3N_2 to MgO, although this capping layer thickness would need to be precisely determined such that one would still be able to obtain useful data from profilometry measurements.

Sample Number	Measurement 1 Thickness	Measurement 2 Thickness	Average Thickness	QCM Thickness
183	119.88 nm	124.87 nm	122.375 nm	1410 nm
185	115.80 nm	122.59 nm	119.195 nm	72.4 nm
187	121.15 nm	121.16 nm	121.155 nm	116.4 nm

Table 5: Thickness results for WN_x calibration growths. Note that updated density and z-ratio information are reflected in sample number 185, and 187 reflects an updated tooling factor of 160%.

The WN_x growths clearly did not experience the same degree of oxidation as their Mg_3N_2 counterparts, thus making the determination of a trustworthy average thickness much more feasible. Total film thickness of all six measurements was averaged at the end to yield an updated tooling factor of 165%, and a final test was performed with that updated parameter which revealed an average deposition rate of 0.31 Å/s for the Q gun.

A VESTA visualization of $MgWN_2$ in our desired ordered layered "rocksaline" crystal structure (space group $P6_3/mmc$, No. 194) was created, as shown in Figure 3. We determined the layer thickness for the ordered rocksaline crystal structure to be 2.6375 Å[2,8]. Using the previously determined 0.31 Å/s deposition rate for WN_x, it was determined that the W shutter would need to be open for approximately 9 seconds to produce the desired layer thickness. The Mg shutter time was chosen to be approximately 8 seconds, as the Mg_3N_2 deposition rate tended to be slightly higher than that of WN_x.

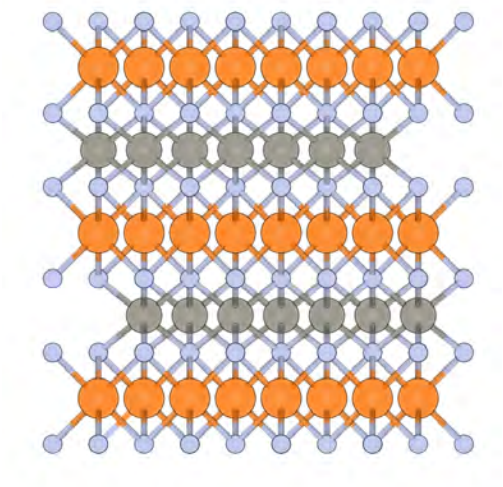

Figure 3: Diagram of the predicted ordered "rocksaline" crystal structure of $MgWN_2$, showing layers of Mg and W bonded to nitrogen atoms. Figure created in VESTA molecular visualization software[2].

B. Synthesis of $MgWN_2$

1. Non-Layered Synthesis of $MgWN_2$

Initial non-layered $MgWN_2$ films were produced in an attempt to replicate the previously-reported novel rocksaline crystal structure, which has been successfully grown by RF sputtering in another deposition chamber at NREL followed by ex-situ annealing in flowing N_2 at 900 °C[8]. The films grown in this study were then analyzed with XRD and XRF, as shown in Figure 4.

The XRD data of the as-grown films reveal a purely rocksalt crystal structure, which is not entirely unexpected as the rocksaline structure did not emerge until the sample was annealed at 900 °C in previous work[8]. We note that that no sign of the AlN capping layer

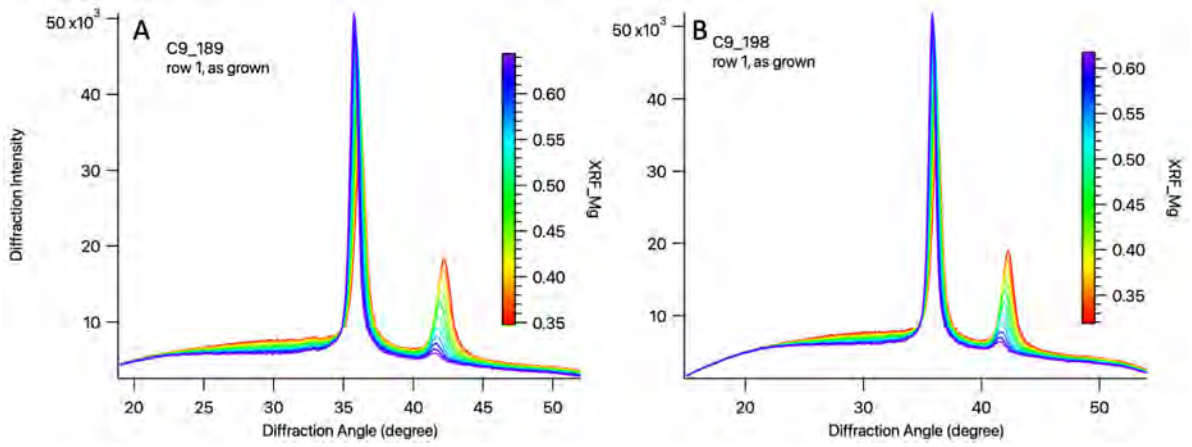

Figure 4: XRD data of non-layered, ambient temperature growths of $MgWN_2$ on different substrates. A) XRD data of a film grown on a pSi(100) substrate. B) XRD data of a film grown on a SiN_x | Si substrate, with an AlN capping layer (30 min deposition). The curve color corresponds to the Mg content in % Mg/(Mg+W), as measured by XRF.

is seen in the XRD data, implying that this layer must be either very thin or amorphous, or both.

i. Annealing studies of non-layered growths

Ex-situ rapid thermal annealing (RTA) studies in flowing N_2 were performed on two non-layered $MgWN_2$ films. For each film, anneals were performed at 600 °C and 900 °C, and either 800 °C or 1000 °C, on separate rows of the sample library. The resulting XRD data are shown in Figures 5 and 6.

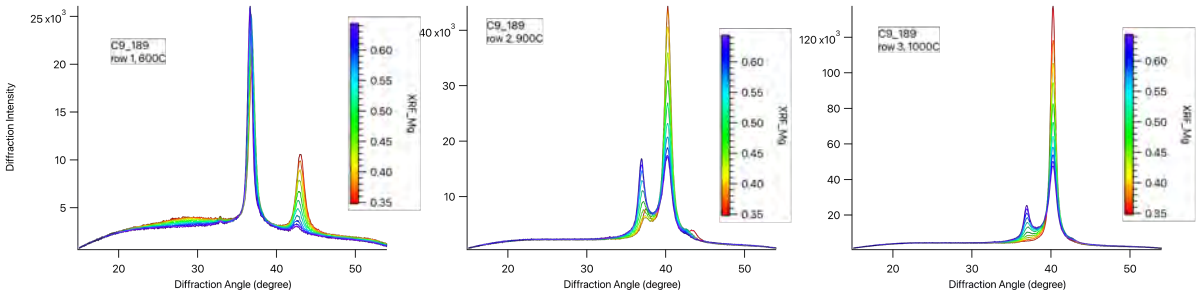

Figure 5: XRD data for RTA studies performed on a non-layered $MgWN_2$ film grown on a pSi(100) substrate. A) Annealed at 600 °C. B) Annealed at 900 °C. C) Annealed at 1000 °C. The curve color corresponds to the Mg content in % Mg/(Mg+W), as measured by XRF.

With the pSi(100) substrate (Figure 5) the results at 600 °C are a rocksalt as expected, which is the same as the non-annealed sample. At higher anneal temps (Figure 5B-C) metallic W begins to form as indicated by the 2θ=40deg peak. The 900 °C anneal exhibits a mixture of rocksalt and W, while at 1000 °C there is even more rocksalt and less W. To

counteract some of these effects we performed the same RTA on a film grown on SiN_x | Si substrate with an AlN capping layer which should both protect the $MgWN_2$ film from oxidation and from other reactions during the annealing process. Unfortunately, the same behavior of forming metallic W with decreasing rocksalt is exhibited for this second film as well.

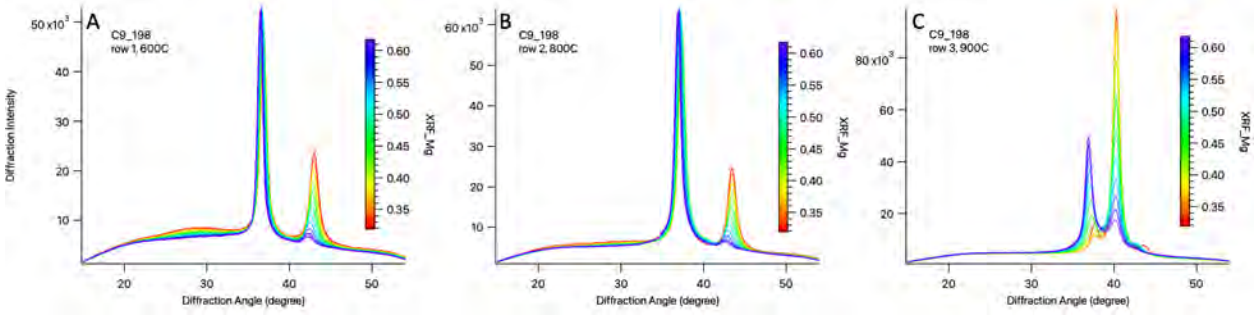

Figure 6: XRD data for RTA studies performed on a non-layered $MgWN_2$ film grown on a SiN_x | Si substrate, with an AlN capping layer (30 min deposition). A) Annealed at 600 °C. B) Annealed at 900 °C. C) Annealed at 1000 °C. The curve color corresponds to the Mg content in % Mg/(Mg+W), as measured by XRF.

2. Layered Synthesis of $MgWN_2$

Here we implement the layered shutter program using the calibrated shutter times in an effort to target the layered rocksaline $MgWN_2$. We initially chose to run 400 cycles of 8s Mg 9s W, which tended to produce an ideal 50-50 composition in the middle of the substrate while simultaneously producing a film thick enough to be reliably measured by XRD.

In an attempt to explore how different deposition parameters influenced the potential formation of the rocksaline crystal structure, we performed a series of growths in which we increased substrate temperature to 200 °C and 400 °C, as referenced in Figure 7.

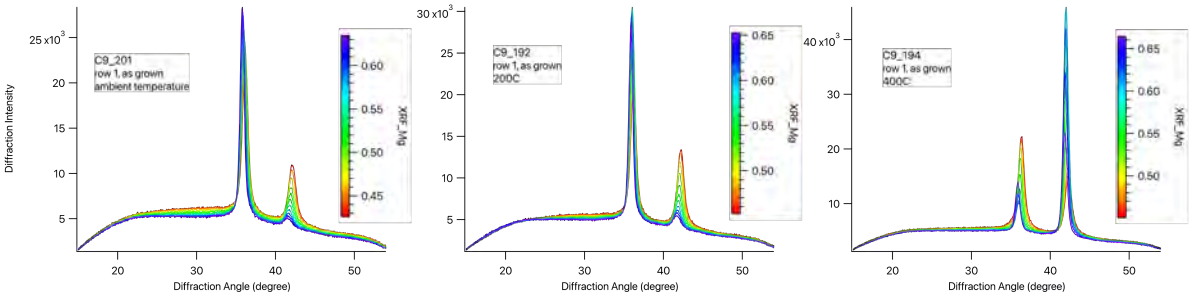

Figure 7: XRD data for a substrate temperature series performed on layered $MgWN_2$ films on pSi(100) substrates. All depositions were performed in a layered manner, with 8 s Mg shutter times and 9 s W shutter times. A) Deposited on substrate at ambient temperature. B) Deposited on substrate at 200 °C. C) Deposited on substrate at 400 °C. The curve color corresponds to the Mg content in % Mg/(Mg+W), as measured by XRF.

XRD data revealed that this temperature series made little difference in the crystal structure: all films exhibited strong rocksalt behavior, with peaks located at 36° and 42° as found in previous diffraction patterns.

We then explored producing layered films on SiN_x | Si with an AlN capping layer as in the non-layered growths, to reduce the likelihood of oxidation as well as any other adverse reactions from occurring during deposition or annealing.

Here we see little difference between the film grown on SiN_x | Si when compared to pSi(100). We note that, similar to the behavior seen in the non-layered growths (Figures 4–6), no peaks from the AlN capping layer are visible in the XRD data, implying that this layer is either very thin or amorphous, or both.

As we did not see any evidence of the rocksaline structure in our ambient-temperature layered growths (Figures 7–8), we used XRR to check for the presence of any material layering: it would correspond to the appearance of a Bragg peak in the XRR data (Figure 9).

Unfortunately, the lack of Bragg peaks in the XRR data (Figure 9) implies no material layering for a film deposited with 100 cycles of 8 s Mg and 9 s W shutter times. However, the presence of the oscillations (known as Kiessing fringes) confirms that the film is present, thin, and that interface between the substrate and the film is not overly rough. Additionally, the gradual decrease in intensity over the measured 2θ range indicates that the film surface is smooth enough to yield high-quality XRR data. To explore further, we experimented with

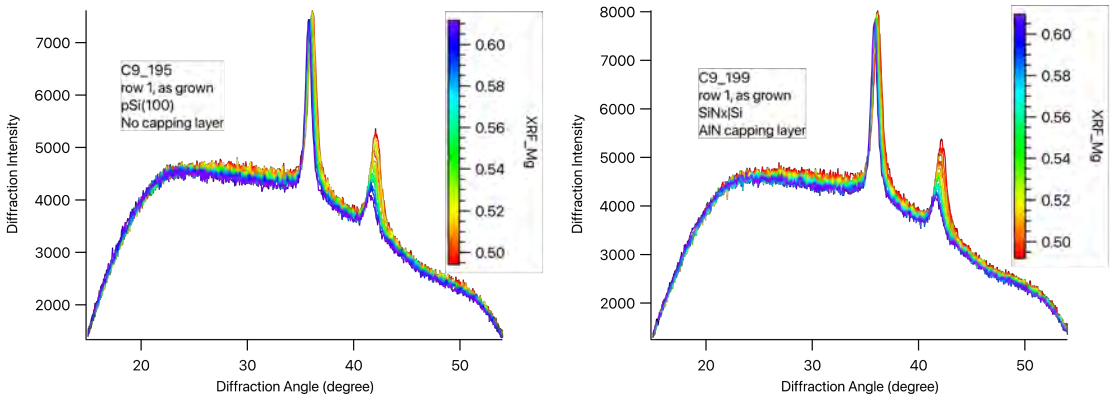

Figure 8: XRD data comparing A) a layered growth on pSi(100) without a capping layer and B) a layered growth on SiN_x | Si substrate with a 30 minute AlN capping layer both as deposited. The curve color corresponds to the Mg content in % Mg/(Mg+W), as measured by XRF.

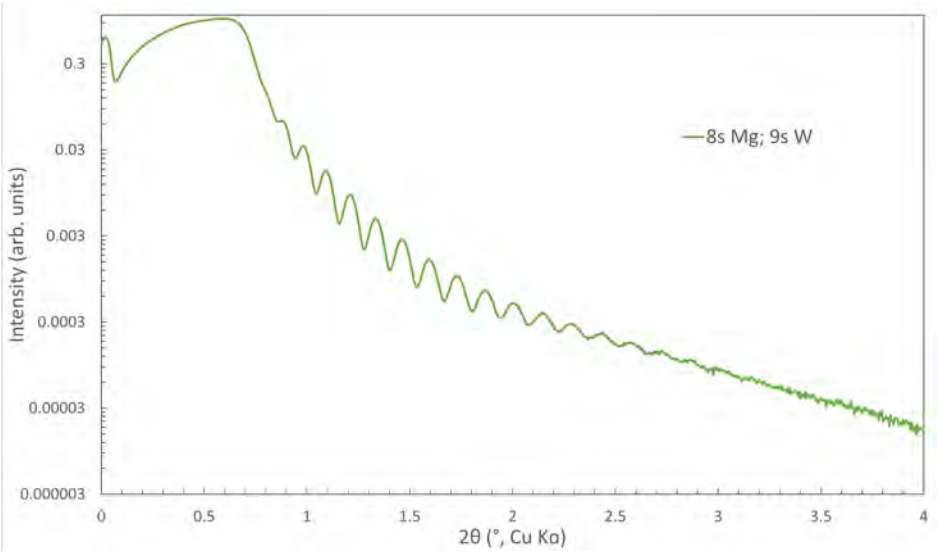

Figure 9: XRR data for a 100 cycle 8 s Mg / 9 s W shutter deposition from $2\theta = 0 - 4°$ showing no layering (as indicated by the lack of any Bragg peaks).

varying the shutter times more substantially to see how that would impact crystal structure and possible material layering.

XRD data (Figure 10) revealed no change in crystalline structure with varying shutter times for as-grown samples; all samples exhibit a rocksalt structure. Therefore, a similar annealing study was performed to explore if heating the sample to 600 °C, 800 °C or 900 °C would induce a structural phase transition, for instance to the layered rocksaline structure.

i. Annealing studies of layered growths

Several annealing studies were performed on these layered growths with varied shutter

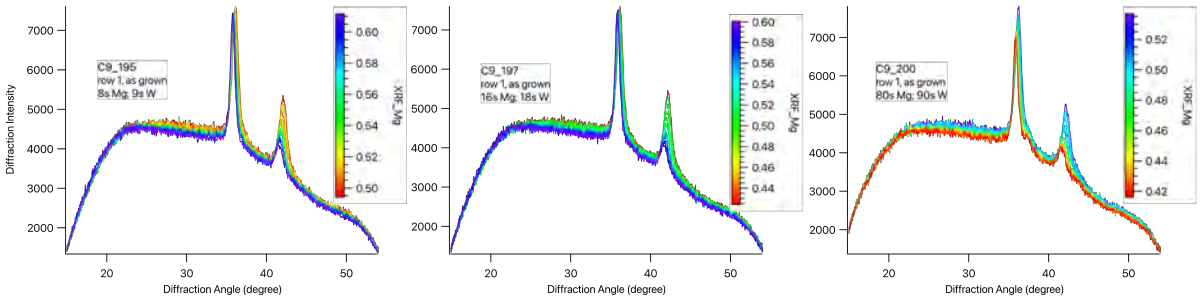

Figure 10: XRD data for layered films deposited with varying shutter times of A) 8s Mg / 9s W. B) 16s Mg / 18s W. C) 80s Mg / 90s W. The curve color corresponds to the Mg content in % Mg/(Mg+W), as measured by XRF.

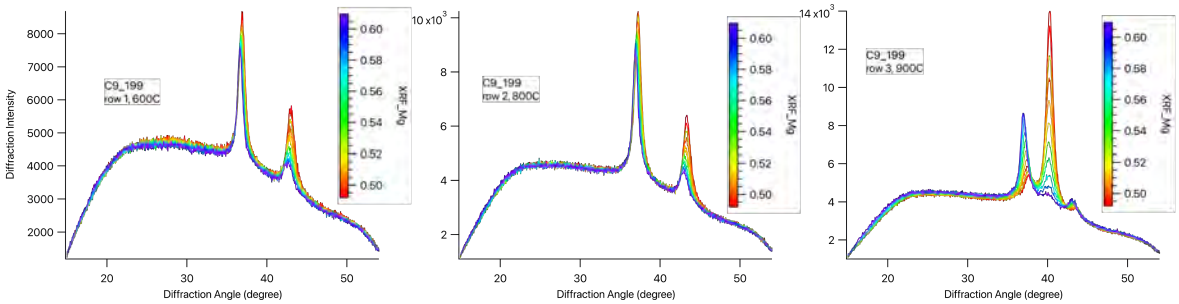

Figure 11: XRD data for annealing studies performed on a layered $MgWN_2$ film with 8s Mg and 9s W shutter times grown on a SiN_x | Si substrate, with an AlN capping layer (30 min deposition). A) Annealed at 600 °C. B) Annealed at 800 °C. C) Annealed at 900 °C. The curve color corresponds to the Mg content in % Mg/(Mg+W), as measured by XRF.

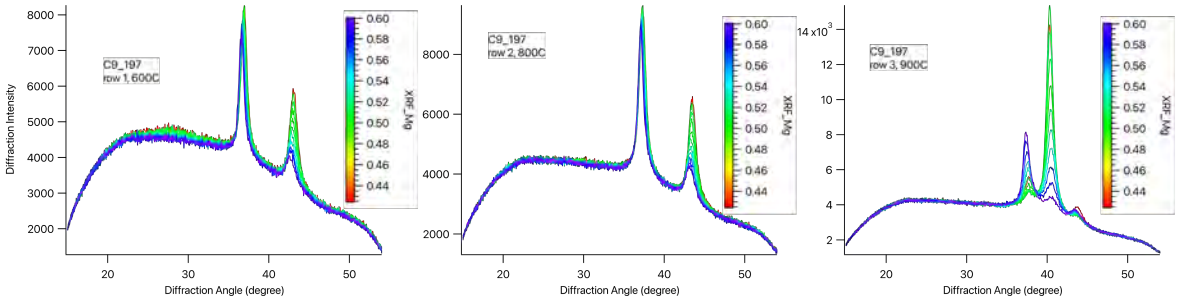

Figure 12: XRD data for annealing studies performed on a layered $MgWN_2$ film with 16s Mg and 18s W shutter times grown on a pSi(100) substrate. A) Annealed at 600 °C. B) Annealed at 800 °C. C) Annealed at 900 °C. The curve color corresponds to the Mg content in % Mg/(Mg+W), as measured by XRF.

times of 8s Mg 9s W, 16s Mg 18s W, and 80s Mg and 90s W to explore whether thicker material layers would have any influence on the overall crystallinity of the film. A similar annealing procedure was performed as on the earlier films, with samples heated under flowing N_2 at 600 °C, 800 °C, and 900 °C for 3 minutes. XRD results of these annealed films indicated

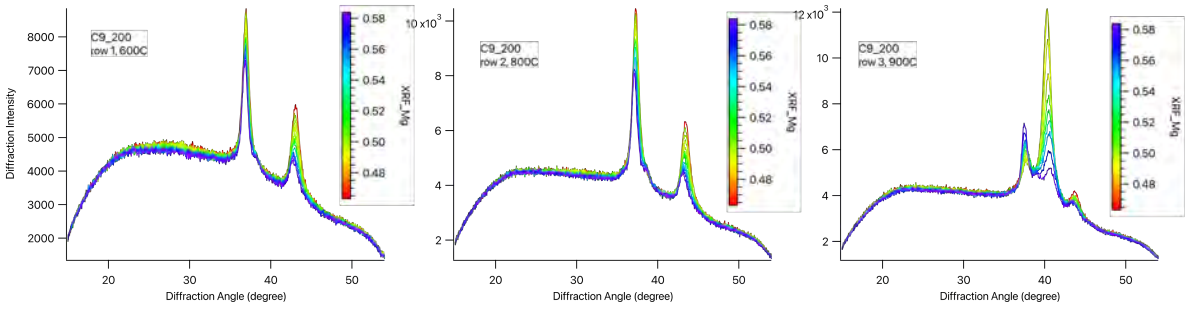

Figure 13: XRD data for annealing studies performed on a layered $MgWN_2$ film with 80s Mg and 90s W shutter times grown on a pSi(100) substrate. A) Annealed at 600 °C. B) Annealed at 800 °C. C) Annealed at 900 °C. The curve color corresponds to the Mg content in % Mg/(Mg+W), as measured by XRF.

further rocksalt structure, with metallic W emerging at high anneal temps as seen in Figure 5.

Unfortunately, no material layering was seen via XRR from the initial, short-shutter layered films as-grown (Figure 9), nor was there any indication of the rocksaline structure being present in the numerous annealed layered and non-layered films. While there are many factors likely contributing to our inability to reproduce this novel rocksaline structure that would be worthwhile to explore, the focus of this research shifted instead towards verifying the existence of material layering of any kind. This was explored through the deposition of thin films with widely-varied shutter times, as described below.

3. Verification of Material Layering

XRR analysis was performed on numerous thin layered growths with shutter times ranging from 8 s Mg / 9 s W to 80 s Mg / 90 s W, as indicated in Figure 14.

The XRR data reveal Bragg peaks indicative of a layered superstructure for samples with shutter times as low as 32 s Mg / 36 s W. Modeling performed on the 80 s Mg / 90 s W $MgWN_2$ growth indicated layer thicknesses of approximately 2.5 nm, consistent with the fact that the original desired thickness with 8 s Mg / 9 s W shutter times was approximately 2.5 Å. Therefore, with 80 s Mg / 90 s W shutter times producing roughly 2.5 nm thick layers, one can reasonably extrapolate that the layer thickness from 32 s Mg / 36 s W shutter times would be around 1 nm. While this is still several times greater than the desired thickness of 2.5 Å, it is valuable to know that at the deposition conditions used for these growths, 1 nm thick layers is approximately as thin as one can go before the layering is no longer detectable by XRR.

IV. CONCLUSIONS AND FUTURE RESEARCH

While we were ultimately unable to reproduce the atomically-layered rocksaline crystal structure as originally hoped, XRR data confirmed the presence of material layering that occurred as a result of the layered shutter program operating on the sputtering chamber. This is an exciting proof-of-concept for this new chamber, and it opens the door for significant

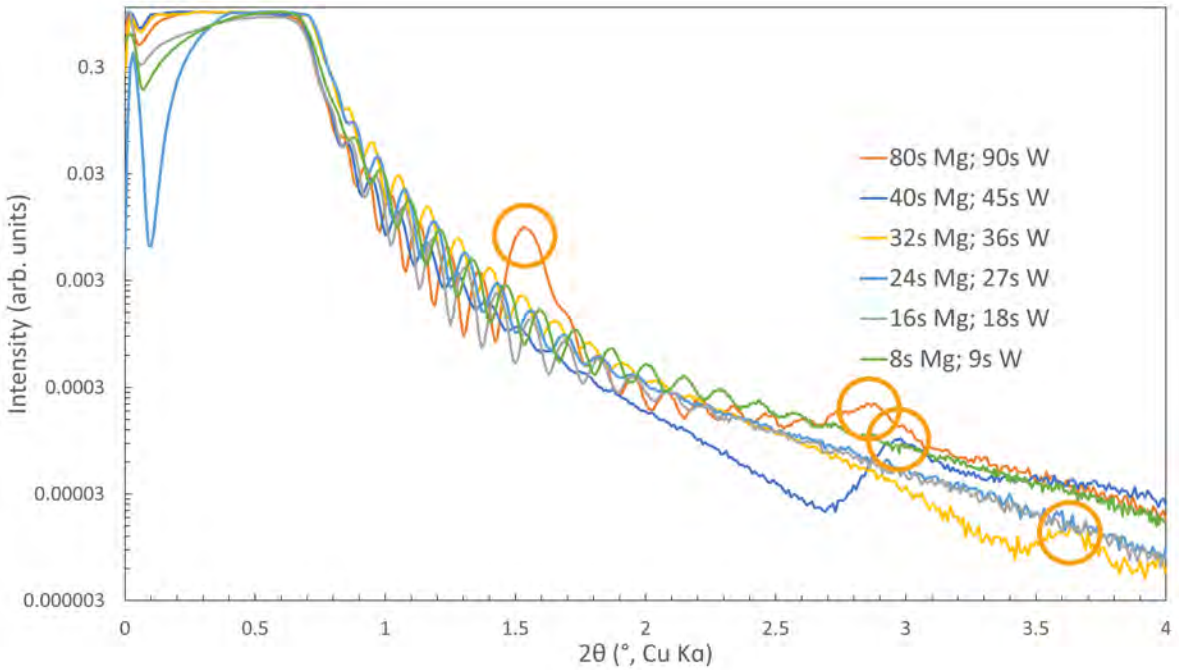

Figure 14: XRR data for layered growths with varied shutter times, all deposited at ambient temperature on a pSi(100) substrate. Note the Bragg peaks circled in orange.

future research into gradually decreasing the layer thickness able to be produced through sputtering.

Future research will explore modifying numerous deposition parameters, especially substrate temperature, gun power, and chamber pressure to produce thinner material layers. The atoms being deposited during sputtering have extremely high kinetic energy, resulting in frequent impingement as these atoms either embed themselves into earlier layers of material or fail to adhere to the substrate to begin with. Installing a liquid nitrogen cooling stage for the substrate would allow the deposited atoms to be "trapped" upon contact with the substrate, rapidly decreasing their energy and reducing the likelihood of impingement or other complications to deposition. Additionally, decreasing gun power would significantly decrease the energy of the incoming atoms further decreasing these effects. Lastly, increasing chamber pressure would increase the number of intermediate particle collisions further reducing overall kinetic energy, with the eventual goal of reducing atom energy enough to allow for the desired atomic-level layered deposition.

V. ACKNOWLEDGMENTS

I would like to thank my mentor, Rebecca Smaha, for giving me time and patience as I explored this project. I would also like to thank Davi Febba, whose support with the sputtering chamber was crucial to the success of this research. Sage Bauers, Dennice Roberts, John Mangum, Annie Greenaway, Chris Rom and Andriy Zakutayev all provided their time and insight which helped me as I progressed through this project.

VI. REFERENCES

[1] A. K. Geim and I. V. Grigorieva. "Van der Waals heterostructures". In: *Nature* 499 (7459 2013), pp. 419–425. ISSN: 00280836. DOI: 10.1038/nature12385.

[2] Koichi Momma and Fujio Izumi. "*VESTA3* for three-dimensional visualization of crystal, volumetric and morphology data". In: *Journal of Applied Crystallography* 44.6 (Dec. 2011), pp. 1272–1276. DOI: 10.1107/S0021889811038970. URL: https://doi.org/10.1107/S0021889811038970.

[3] K S Novoselov et al. *Electric Field Effect in Atomically Thin Carbon Films*. 2000, p. 3824. URL: www.arXiv.org/quant-ph/.

[4] K. S. Novoselov et al. "2D materials and van der Waals heterostructures". In: *Science* 353 (6298 July 2016). ISSN: 0036-8075. DOI: 10.1126/science.aac9439.

[5] Dennice M. Roberts et al. "Amorphous sulfide heterostructure precursors prepared by radio frequency sputtering". In: *Journal of Vacuum Science & Technology B* 37 (5 Sept. 2019), p. 051201. ISSN: 2166-2746. DOI: 10.1116/1.5099502.

[6] Dennice M. Roberts et al. "Synthesis of Tunable SnS-TaS2Nanoscale Superlattices". In: *Nano Letters* 20 (10 Oct. 2020), pp. 7059–7067. ISSN: 15306992. DOI: 10.1021/acs.nanolett.0c02115.

[7] Kevin R. Talley et al. "COMBIgor: Data-analysis package for combinatorial materials science". In: *ACS Combinatorial Science* 21.7 (2019), pp. 537–547. ISSN: 21568944. DOI: 10.1021/acscombsci.9b00077.

[8] Andriy Zakutayev, Sage R. Bauers, and Stephan Lany. "Experimental Synthesis of Theoretically Predicted Multivalent Ternary Nitride Materials". In: *Chemistry of Materials* 34 (4 Feb. 2022), pp. 1418–1438. ISSN: 15205002. DOI: 10.1021/acs.chemmater.1c03014.